ORIGINAL ARTICLE

Diagnostic value of tumor blood flow and its histogram analysis obtained with pCASL to differentiate sinonasal lymphoma from squamous cell carcinoma

Noriyuki Fujima, MD, PhD[1]; Hiroyuki Kameda, MD[1]; Akiko Tsukahara, MD[1]; Daisuke Yoshida, MD[1]; Tomohiro Sakashita, MD, PhD[2]; Akihiro Homma, MD, PhD[2]; Khin Khin Tha, MD, PhD[3,4]; Kohsuke Kudo, MD, PhD[1]; and Hiroki Shirato, MD, PhD[3,4]

[1] Department of Diagnostic and Interventional Radiology, Hokkaido University Hospital, Sapporo, Japan

[2] Department of Otolaryngology-Head and Neck Surgery, Hokkaido University Graduate School of Medicine, Sapporo, Japan

[3] Department of Radiation Medicine, Hokkaido University Graduate School of Medicine, Sapporo, Japan

[4] The Global Station for Quantum Medical Science and Engineering, Global Institution for collaborative research and education, Sapporo, Japan

Corresponding Author

Noriyuki Fujima

Department of Diagnostic and Interventional Radiology, Hokkaido University Hospital

N15, W7, Kita-Ku, Sapporo 060-8638, Japan

Phone: +81-11-706-5977, Fax: +81-11-706-7876

E-mail: Noriyuki.Fujima@mb9.seikyou.ne.jp

Original Research

Diagnostic value of tumor blood flow and its histogram analysis obtained with pCASL to differentiate sinonasal malignant lymphoma from squamous cell carcinoma

ABSTRACT

Objectives: To investigate the diagnostic value of tumor blood flow (TBF) obtained with pseudo-continuous arterial spin labeling (pCASL) for the differentiation of squamous cell carcinoma (SCC) and malignant lymphoma (ML) in the nasal or sinonasal cavity.

Methods: Thirty-three patients with SCC and six patients with ML in the nasal or sinonasal cavity were retrospectively analyzed. Quantitative TBF values were obtained using whole-tumor region of interest (ROI) from pCASL data. The histogram analysis of TBF values within the tumor ROI was also performed by calculating the coefficient of variation (CV), kurtosis, and skewness. The mean TBF value, histogram CV, kurtosis and skewness of the patients with SCC were compared with those of the ML patients. The diagnostic accuracy to differentiate SCC from ML was also calculated by receiver operating characteristic (ROC) curve analysis. In addition, multiple logistic regression models were also performed to determine their independent predictive value, and diagnostic accuracy with the combined use of these parameters.

Results: Between the SCC and ML groups, significant differences were observed in mean TBF, CV, and kurtosis, but not in skewness. In ROC curve analysis, the diagnostic accuracy values for the differentiation of SCC from ML in mean TBF, CV, and kurtosis

were all 0.87, respectively. Multiple logistic regression models revealed TBF and CV were respectively independent predictive value. With the combination of these parameters, the diagnostic accuracy was elevated to 0.97.

Conclusions: The TBF value and its histogram analysis obtained with pCASL can help differentiate SCC and ML.

Keywords: Tumor blood flow, pseudo-continuous arterial spin labeling, squamous cell carcinoma, malignant lymphoma

Abbreviations

ADC: apparent diffusion coefficient

AUC: area under curve

CT: computed tomography

CV: coefficient of variation

DCE: dynamic contrast-enhanced

DWI: diffusion-weighted imaging

FOV: field of view

ML: malignant lymphoma

MRI: magnetic resonance imaging

pCASL: pseudo-continuous arterial spin labeling

ROC: receiver operating characteristic

ROI: region of interest

SCC: squamous cell carcinoma

T1WI: T1-weighted image

T2WI: T2-weughted image

TBF: tumor blood flow

TSE: turbo spin-echo

INTRODUCTION

Squamous cell carcinoma (SCC) is the most common tumor among nasal and sinonasal cavity malignancies [1]. Treatments for SCC include surgical treatment, chemotherapy, radiotherapy, and combinations of these [2]. Malignant lymphoma (ML) is the most common malignancy among non-epithelial sinonasal neoplasms, and it is especially frequent in Asian populations [3, 4]. Unlike SCC, the standard methods of treatment for ML do not include surgical treatment, and the chemotherapy regimen for ML is quite different from that used for SCC, in which cisplatin is usually used [5].

The differentiation of SCC and ML is required in many cases. The histopathological findings are the gold standard for the diagnoses of both SCC and ML. However, a surgical biopsy sometimes misses the diagnosis because tissue containing the tumor cells is not always obtained; peripheral inflammatory tissue (especially concomitant or simultaneous inflammation) is commonly observed in the nasal or sinonasal cavity [6]. For this reason, other methods to assist the diagnosis of SCC or ML are desired.

The differentiation of SCC and ML by only conventional computed tomography (CT) or magnetic resonance imaging (MRI) such as T1-weighted images (T1WI), T2-weughted images (T2WI) and post-contrast-enhanced images has been described as

difficult [7]. Diffusion-weighted imaging (DWI) was reported to be useful in the differentiation of SCC and ML for the evaluation of the primary site or lymph nodes by using the apparent diffusion coefficient (ADC), which is reported to reflect the physiological parameter of tissue cellular density [8-11]. A tendency for lower ADC values in MLs compared to that in SCCs was reported, but the diagnostic performance of the ADCs was not adequate, and several cases overlapped between SCC and ML [8-10]. In contrast, tumor perfusion can be useful for the differential diagnosis of SCC and ML as another physiological parameter. Dynamic contrast-enhanced (DCE) perfusion techniques that were reported to be useful for this differentiation use the pattern of the dynamic curve of the tumor concentration of the contrast agent, or the perfusion-related parameters of k-trans, plasma volume, and the volume of extracellular space [12-14]. A pseudo-continuous arterial spin labeling (pCASL) technique is now widely used for the noninvasive measurement of tissue blood flow by using protons in arterial water as the intrinsic tracer [15]. The reliability of pseudo-continuous arterial spin labeling for use in head and neck tumors was recently described [16]. Unlike DCE perfusion, pCASL can be performed noninvasively without contrast agent, and its blood flow measurements might be more accurate because the tracer in ASL is more diffusible than the contrast agent in MR Perfusion (gadolinium chelate) [17].

The aim of the present study was to investigate the diagnostic value of tumor blood flow (TBF) obtained with pCASL for the differentiation of SCC and ML in the nasal or sinonasal cavity.

MATERIALS AND METHODS

Patients

The study protocol was approved by our institutional review board. The cases of 33 patients with SCC and six patients with ML in the nasal or sinonasal cavity were evaluated retrospectively with the following inclusion criteria: (1) the patient was first diagnosed (not a recurrent case) histopathologically as having SCC or ML, and (2) MR scanning was performed before any treatment. The SCC patients were 28 males (mean age 61.8 yrs, range 46–79 yrs) and five females (mean age 59.2 yrs, range 43–89 yrs). The primary sites of the 33 patients with SCC were the maxillary sinus in 29 patients and the nasal cavity in four patients.

The patients with ML were six males (mean age 65.8 yrs, range 52–79 yrs) and no females. The primary sites were the maxillary sinus in two patients, the ethmoid sinus in one patient, and the nasal cavity in three patients.

Imaging parameters

All MR imaging was performed using a 3.0 Tesla unit (Achieva TX; Philips Medical Systems, Best, the Netherlands) with a 16-channel neurovascular coil. First, conventional MR images were obtained to evaluate the primary tumor. These images included (a) axial T1WI with a spin-echo sequence (TR, 450 msec; TE, 10 msec; field of view (FOV), 240×240 mm; 512×512 matrix; slice thickness, 5 mm; inter-slice gap, 30%; scanning time, 2 min 12 s) and (b) axial T2WI with a turbo spin-echo (TSE) sequence with fat suppression (TR, 4500 msec; TE, 70 msec; TSE factor, 9; FOV, 240×240 mm; 512×512 matrix; slice thickness, 5 mm; inter-slice gap, 30%; scanning time, 2 min 6 s).

In the pCASL scanning, coronal T2WI was performed to obtain anatomical information of the carotid artery for the positioning of the labeling slab. A T1 map was also obtained to measure the longitudinal relaxation in the tumor tissue, and it was used for the TBF quantification. The acquisition of pCASL was performed by using multi-shot spin-echo echo-planar imaging to obtain control and labeled images. The labeling slab was placed just under the bifurcation of the internal and external carotid arteries by using coronal T2WI as a reference.

The MR parameters of the pCASL were as follows: labeling duration, 1650 msec;

post-label delay, 1280 msec; TR, 3619 msec; TE, 18 msec; flip angle, 90°; number of shots, two; FOV, 230×230 mm; matrix, 80×80; slice thickness, 5 mm; number of slices, 15; acceleration factor for parallel imaging, two; and scanning time, 5 min 11 s. The patients were instructed not to swallow, move their tongues, open their mouths, or make any other voluntary motion during the pCASL scan. In addition, their heads were fixed firmly with the coil to prevent movement during the scan.

The coronal T2WI was obtained by TSE sequence with the following parameters: TR, 4500 msec; TE, 70 msec; TSE factor, 9; FOV, 240×240 mm; matrix, 512×512; slice thickness, 4 mm; inter-slice gap, 30%; scanning time, 2 min 6 s. For the T1 map, a gradient echo sequence with the Look-Locker readout and a constant flip angle was used with the following parameters: TR, 7 msec; TE, 1.7 msec; flip angle, 7°; FOV, 230×230 mm; matrix, 256×256; slice thickness, 10 mm (single slice acquisition); scanning time, 6 s.

Data analysis

TBF calculation by pCASL

We calculated the TBF of the pCASL (f) from the signal difference (ΔM), which was calculated by subtracting the labeled image from the control image, using the

previously described equation [18]:

$$f = \frac{\Delta M \lambda R_{1a} \exp(\omega R_{1a})}{2M_0 \alpha}[1 - \exp(-\gamma R_{1a})]^{-1} \quad [1]$$

where R_{1a} is the longitudinal relaxation rate of blood (0.67 s^{-1}), γ is the labeling time (1.65 s), ω is the post-labeling delay time (1.28 s), α is the labeling efficiency (0.85), and λ is the blood/tumor-tissue water partition coefficient (1.0 g/mL) [19, 20]. M_0 is the equilibrium magnetization of the tumor tissue, which was estimated from the signal intensity of the control image and the tumor longitudinal relaxation rate obtained by the T1 map. Using Eq. [1], we created the TBF maps on a pixel-by-pixel basis. We used Mathematical software (MATLAB, ver. 2012a) to calculate the TBF values for the pCASL.

Tumor ROI delineation and quantification

The primary tumor in both the SCCs and MLs was outlined by a board-certified neuroradiologist with 18 years of experience (A.T.), blinded to the histopathological diagnosis. The delineation was performed on the axial T2WI with a polygonal region of interest (ROI), and the ROI was then copied onto a TBF map (Fig. 1). T1WI was also used as a guide to determine the ROI. To avoid vascular artifacts in the ROI, the area of

the vessel signal void was also delineated on T2WI, and this area was excluded from the TBF measurement. A strong high signal area with T2WI which suggested necrosis was also excluded. The TBF value of pCASL in each patient was determined as the mean of the TBF values in the delineated ROI. If the tumor extended into two or more slices on the TBF map, the mean TBF of all pixels in all ROIs of the tumor was calculated as the TBF value.

A histogram analysis method was performed to assess the distribution of TBF values within each tumor ROI. As with the TBF calculation, if the tumor extended into two or more slices on the TBF map, the TBF values of all pixels in all ROIs of the tumor was used for the histogram analysis. The histogram analysis parameters assessed with this method were the coefficient of variation (CV) and histogram skewness and kurtosis. In this study, CV, skewness and kurtosis were defined as follows:

$$CV = \sigma / \mu$$

$$skewness = \left[1/n * \sum (\chi - \mu)^3 \right] / \sigma^3$$

$$kurtosis = \left[1/n * \sum (\chi - \mu)^4 \right] / \sigma^4 - 3$$

where n is the number of pixels within the tumor ROI, x is the TBF value in each pixel,

μ is the mean of x, and σ is the standard deviation of x. The CV describes the normalized measure of dispersion of TBF values. Histogram skewness describes the skew in the shape of the distribution curve of the TBF values. The kurtosis describes the peak and/or flatness of the curve peak; a more acute peak has higher kurtosis, and a more broadened and/or flattened peak has lower kurtosis [21].

Statistical analysis

As univariate analysis, Mann-Whitney U-test was used to compare mean TBF values, histogram parameters of the CV, skewness, and kurtosis values between the SCC and ML respectively. If a significant difference was observed in a parameter, receiver operating characteristic (ROC) curve were constructed for the calculation of area under curve (AUC), and for the determination of best diagnostic accuracy by using the closest point to the upper left corner of ROC curve in the division of SCC and ML patient. In addition, if a significant difference was obtained for more than two parameters among TBF, CV, skewness, and kurtosis, these parameters were subsequently analyzed by multiple logistic regression models to determine their independent predictive value. If multiple parameters were determined as independent predictor by multiple logistic regression models, we also determined the sensitivity, specificity, and diagnostic

accuracy of the combined use of these parameters so that diagnostic accuracy becomes the highest. A p-value of 0.05 was considered significant. All statistics were performed by using the SPSS version 20 for Windows.

RESULTS

The pCASL scanning, TBF measurement and parameter calculation in the histogram analysis were successfully performed in all 39 patients. In univariate analysis using Mann-Whitney U-test, the mean TBF in the 33 SCC patients (140.6 ± 35.7 mL/100 g/min) was significantly higher than that of the six ML patients (93.8 ± 15.1 mL/100 g/min) ($p<0.001$) (Fig. 2). In the histogram analysis, the CV of the SCC patients (0.45 ± 0.09) was significantly higher than that of the ML patients (0.33 ± 0.04) ($p<0.01$) (Fig. 3). The kurtosis of the SCC patients (−0.47 ± 0.29) was significantly lower than that of the ML patients (−0.18 ± 0.21) ($p<0.01$) (Fig. 4). In contrast, there was no significant difference in skewness between the patients with SCC (0.03± 0.29) and those with ML (0.17± 0.37) ($p=0.27$) (Fig. 5). On ROC curve analysis, AUC, sensitivity, specificity, and accuracy of mean TBF were 0.87, 0.85 (28/33), 0.83 (5/6) and 0.85 (33/39) respectively when the threshold was set at 105 – 106 mL/100 g/min. Those of the CV were 0.87, 0.82 (27/33), 0.83 (5/6), 0.82 (32/39) by setting the

threshold at 0.37. Those of kurtosis were 0.78, 0.64 (21/33), 0.83 (5/6), and 0.67 (26/39) respectively by setting the threshold at -0.39 – -0.40 respectively.

By the multiple logistic regression models, mean TBF ($p<0.05$) and histogram parameter of the CV ($p<0.05$) were respectively determined as independent predictor. With the combination of these parameters, with the threshold of ML set as TBF < 119–134, CV > 0.37, the highest accuracy of 0.97 (38/39) was obtained with 0.97 (32/33) sensitivity and 1.00 (6/6) specificity (Figs. 6, 7).

DISCUSSION

We found that the ML patients had significantly lower mean TBF, higher kurtosis and lower CV by histogram analysis compared to the SCC patients by univariate analysis. Additionally, by the multiple logistic regression models, mean TBF and histogram parameter of the CV were revealed as independent diagnostic parameter for the differentiation of SCC and ML patients. Higher diagnostic accuracy was obtained by combining these two parameters, although the case of only one patient with SCC overlapped in patients group of ML.

We were unable to find any report in the extant literature that describes a

difference in TBF between SCC and ML cases using quantitative values obtained by pCASL. However, several studies investigated tumor perfusion-related parameters by using a DCE technique. Asaumi et al. reported that high peak signal intensity from the dynamic curve after a bolus injection of contrast agent was obtained from most SCCs, whereas 70% of the ML cases did not show such high peak signal intensity in their dynamic curves [14]. Lee et al. reported that the mean plasma volume (which has been related to blood volume) was higher in SCC cases than that in ML cases, although the difference was not significant [12]. These reports indicated that the degree of the tumor perfusion of MLs was lower than that of SCCs. Our present finding of a significant difference in TBF values between SCC and ML shows the same tendency as that described in these earlier reports.

In general imaging findings in conventional MR signal intensity, a tendency for homogeneous signal intensity in ML has been reported [22]. However, homogeneity in the tumor perfusion map was not investigated in the past studies. The present study's ML findings of higher kurtosis and lower CV in the histogram analysis showed a narrow range of TBF map pixel values; this result indicates homogeneous perfusion in most cases of ML compared to SCC. We suspect that one of the main reasons for the heterogeneity in the TBF distribution is the intra-tumoral necrosis in SCCs. Lesions

near tumor necrosis are generally considered hypoxic areas with hypovascularity. In contrast, hypervascularity has been observed frequently in peripheral areas of SCCs [16]. This difference in intra-tumoral vascularity was considered to reflect heterogeneity in the TBF map. Because necrotic areas are less frequently observed in ML, a more homogeneous TBF distribution was observed in the present ML cases compared to the SCC cases.

With the combination of the mean TBF and the histogram parameter of CV, the diagnostic accuracy was better than that obtained with the mean TBF or a histogram analysis parameter alone. The mean TBF values of several patients with ML overlapped with those of several patients with SCC. However, such patients can be differentiated by using the parameters in a histogram analysis. In contrast, for several of our patients with SCC, the histogram analysis revealed homogeneity with higher kurtosis and a lower CV value similar to those of our ML patients, and the cases of these SCC patients were thus difficult to differentiate from ML by histogram parameters alone. However, most of such patients with SCC can be successfully differentiated with an additional evaluation by mean TBF. In light of these findings, the incidence of SCCs with both lower TBF and a homogeneous histogram is considered very rare, and thus, in the present study the combined use of the mean TBF and histogram parameters obtained with a TBF map was

found to be very effective and to have high diagnostic value for the differentiation of SCC and ML.

In the present study, only one SCC was completely overlapped in the area of ML, even though both the mean TBF and its histogram value were respectively used for differentiation. The location of this SCC was the right maxillary sinus, and it was moderately differentiated in histopathological findings. There was no particular information that differed from that of the other SCCs. It remains unclear whether other factors such as the p16, p53, Ki-67 expression or human papilloma virus status are related to the difficulty of the differentiation to ML. Further analyses in a multivariate correlation study are necessary to address this question.

In patients with nasal or sinonasal malignancy such as SCC or lymphoma, it is very important to determine the treatment method as soon as possible. The pCASL diagnostic technique used in the present study can contribute to the quick assessment for a prompt start of treatment by providing information for the diagnosis.

This study has several limitations. First, the number of patients with ML (n=6) was small. However, it may be difficult to match the patient number between ML and SCC cases, since ML patients are less frequently encountered compared to SCC patients. Further studies of larger numbers of ML patients are necessary. In addition, the details

of the distributions of locations differed between the SCCs and MLs. In particular, there was no patient whose SCC was located in the ethmoid sinus, whereas the tumor of one ML patient was located in the ethmoid sinus. The different locations of the lesions can affect the lesions' feeding arteries and may also affect the TBF values. Another subgroup study of a greater number of patients based on the location of the tumors is also needed. Second, a direct comparison of TBF with other parameters was not conducted. As noted above, conventional imaging such as T1WI and T2WI in ML tended to show homogenous intensity [22], and it can be useful for the differentiation of SCC and ML, although it was also reported that this differentiation was difficult by these findings alone [7]. Additionally, an ADC value measured by DWI was reported to be useful to differentiate SCC and ML [8-11]. The determination of additional diagnostic value of TBF can be used to confirm the utility of TBF assessment. Moreover, TBF and ADC are different physiological parameters, because the ADC value reflects mainly the cellular density of tumor tissue. Combining the TBF and the ADC may provide better diagnostic value. Third, it was sometimes difficult to distinguish secondary inflammation tissue around the tumor from the tumor tissue itself, and thus inflammatory tissue may have been present within the tumor ROI in some cases. In such cases, a certain level of error was included in the measured TBF value due to the

mixture of tumor and inflammatory tissue within the ROI, and this may have influenced the results. We nevertheless speculate that a large error did not occur because the signal intensity was generally different between the tumor tissue and inflammatory tissue, which typically presented clearly high signal intensity on T2WI. Forth, inter-observer agreement was not investigated in the present study. The variations of the shape and/or size of the primary tumors outlined by different researchers may have a significant influence on the histogram analysis. To address this concern, an inter-observer agreement analysis should be performed in a future study.

CONCLUSIONS

In conclusion, we found that pCASL can be a useful tool for the differentiation of SCC and ML. In particular, the combined use of both the mean TBF and histogram parameter of CV obtained with the intra-tumoral TBF signal will be effective as a diagnostic tool with high diagnostic accuracy.

REFERENCES

1. Sanghvi S, Khan MN, Patel NR, Yeldandi S, Baredes S, Eloy JA. Epidemiology of sinonasal squamous cell carcinoma: a comprehensive analysis of 4994 patients. Laryngoscope 2014;124(1):76-83.

2. Jegoux F, Metreau A, Louvel G, Bedfert C. Paranasal sinus cancer. Eur Ann Otorhinolaryngol Head Neck Dis 2013;130(6):327-35.

3. Zylka S, Bien S, Kaminski B, Postula S, Ziolkowska M. [Epidemiology and clinical characteristics of the sinonasal malignancies]. Otolaryngol Pol 2008;62(4):436-41.

4. Vidal RW, Devaney K, Ferlito A, Rinaldo A, Carbone A. Sinonasal malignant lymphomas: a distinct clinicopathological category. Ann Otol Rhinol Laryngol 1999;108(4):411-9.

5. Logsdon MD, Ha CS, Kavadi VS, Cabanillas F, Hess MA, Cox JD. Lymphoma of the nasal cavity and paranasal sinuses: improved outcome and altered prognostic factors with combined modality therapy. Cancer 1997;80(3):477-88.

6. Pal I, Gupta A, Sengupta S. An attempt to define the type of biopsy in a sinonasal lesion showing bony erosion. Indian J Otolaryngol Head Neck Surg

2010;62(1):92-5.

7. Liu XW, Xie CM, Mo YX, Zhang R, Li H, Huang ZL, et al. Magnetic resonance imaging features of nasopharyngeal carcinoma and nasopharyngeal non-Hodgkin's lymphoma: are there differences? Eur J Radiol 2012;81(6):1146-54.

8. Ichikawa Y, Sumi M, Sasaki M, Sumi T, Nakamura T. Efficacy of diffusion-weighted imaging for the differentiation between lymphomas and carcinomas of the nasopharynx and oropharynx: correlations of apparent diffusion coefficients and histologic features. AJNR Am J Neuroradiol 2012;33(4):761-6.

9. Sumi M, Nakamura T. Diagnostic importance of focal defects in the apparent diffusion coefficient-based differentiation between lymphoma and squamous cell carcinoma nodes in the neck. Eur Radiol 2009;19(4):975-81.

10. Sumi M, Ichikawa Y, Nakamura T. Diagnostic ability of apparent diffusion coefficients for lymphomas and carcinomas in the pharynx. Eur Radiol 2007;17(10):2631-7.

11. Razek AA. Diffusion-weighted magnetic resonance imaging of head and neck. J Comput Assist Tomogr 2010;34(6):808-15.

12. Lee FK, King AD, Ma BB, Yeung DK. Dynamic contrast enhancement magnetic resonance imaging (DCE-MRI) for differential diagnosis in head and neck cancers. Eur J Radiol 2012;81(4):784-8.

13. Matsuzaki H, Hara M, Yanagi Y, Asaumi J, Katase N, Unetsubo T, et al. Magnetic resonance imaging (MRI) and dynamic MRI evaluation of extranodal non-Hodgkin lymphoma in oral and maxillofacial regions. Oral Surg Oral Med Oral Pathol Oral Radiol 2012;113(1):126-33.

14. Asaumi J, Yanagi Y, Konouchi H, Hisatomi M, Matsuzaki H, Kishi K. Application of dynamic contrast-enhanced MRI to differentiate malignant lymphoma from squamous cell carcinoma in the head and neck. Oral Oncol 2004;40(6):579-84.

15. Telischak NA, Detre JA, Zaharchuk G. Arterial spin labeling MRI: Clinical applications in the brain. J Magn Reson Imaging 2014; DOI:10.1002/jmri.24751.

16. Fujima N, Kudo K, Tsukahara A, Yoshida D, Sakashita T, Homma A, et al. Measurement of tumor blood flow in head and neck squamous cell carcinoma by pseudo-continuous arterial spin labeling: Comparison with dynamic contrast-enhanced MRI. J Magn Reson Imaging 2014; DOI:10.1002/jmri.24637.

17. Fujima N, Kudo K, Yoshida D, Homma A, Sakashita T, Tsukahara A, et al. Arterial spin labeling to determine tumor viability in head and neck cancer before and after treatment. Journal of magnetic resonance imaging. J Magn Reson Imaging 2014;40(4):920-8.

18. Wang Z, Aguirre GK, Rao H, Wang J, Fernandez-Seara MA, Childress AR, et al. Empirical optimization of ASL data analysis using an ASL data processing toolbox: ASLtbx. Magn Reson Imaging 2008;26(2):261-9.

19. Golay X, Petersen ET, Hui F. Pulsed star labeling of arterial regions (PULSAR): a robust regional perfusion technique for high field imaging. Magn Reson Med 2005;53(1):15-21.

20. Wheeler RH, Ziessman HA, Medvec BR, Juni JE, Thrall JH, Keyes JW, et al. Tumor blood flow and systemic shunting in patients receiving intraarterial chemotherapy for head and neck cancer. Cancer Res 1986;46(8):4200-4.

21. King AD, Chow KK, Yu KH, Mo FK, Yeung DK, Yuan J, et al. Head and neck squamous cell carcinoma: diagnostic performance of diffusion-weighted MR imaging for the prediction of treatment response. Radiology 2013;266(2):531-538.

22. Negendank WG, al-Katib AM, Karanes C, Smith MR. Lymphomas: MR imaging

contrast characteristics with clinical-pathologic correlations. Radiology 1990;177(1):209-16.

Figure Legends

Fig. 1. Tumor ROI delineation.

A sample case (61-yr-old male, right maxillary cancer) of ROI delineation. (a) The tumor was delineated on the axial T2WI with a polygonal ROI. (b) After the delineation, the ROI was copied to the corresponding TBF map.

(a)

(b)

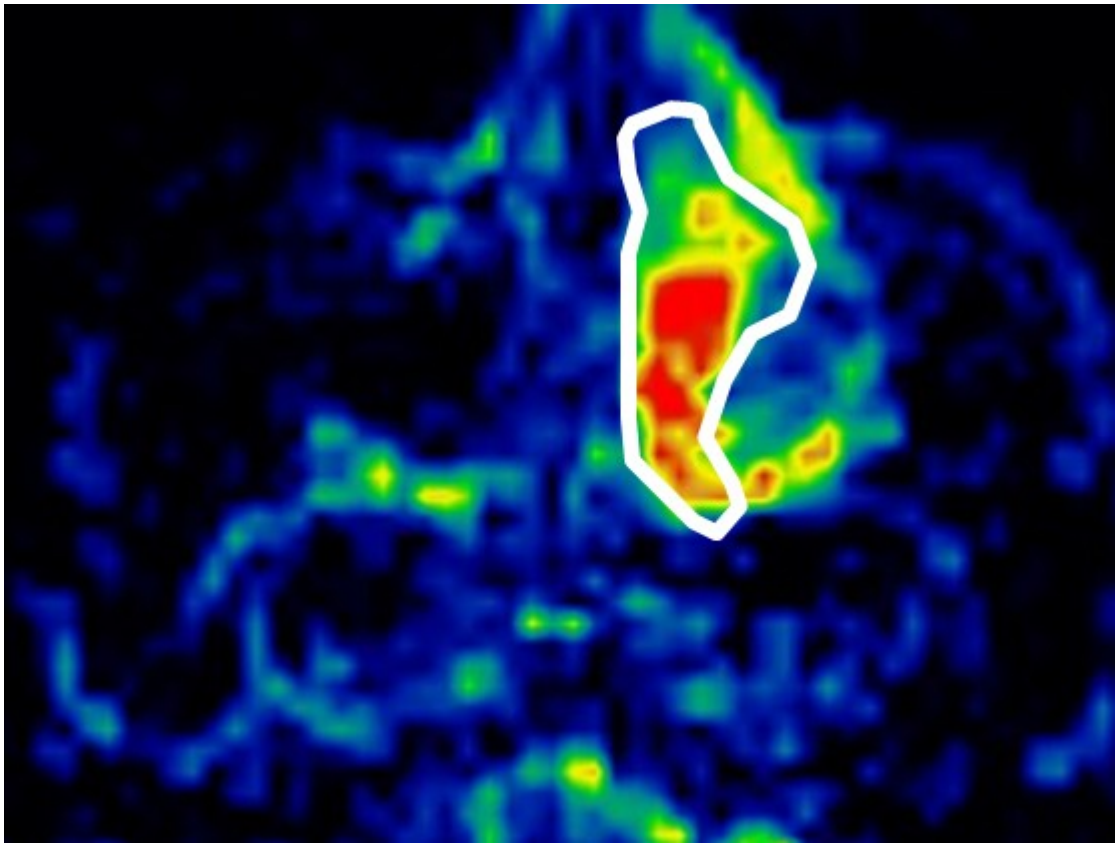

Fig. 2. The TBF in the SCC patients and ML patients.

(a) TBF in patients with SCC or ML. (b) ROC curve for the determination of diagnostic accuracy. The TBF in the 33 patients with SCC (140.6 ± 35.7 mL/100 g/min) was significantly higher than that in the six patients with ML (93.8 ± 15.1 mL/100 g/min) ($p>0.001$) (a, *). The ROC curve analysis revealed the AUC of 0.87 ($p<0.01$) (b), with the best diagnostic accuracy of 0.85 (33/39), sensitivity of 0.85 (28/33), and specificity of 0.83 (5/6), with a threshold value of 105 - 106 mL/100g/min (a, **).

(a)

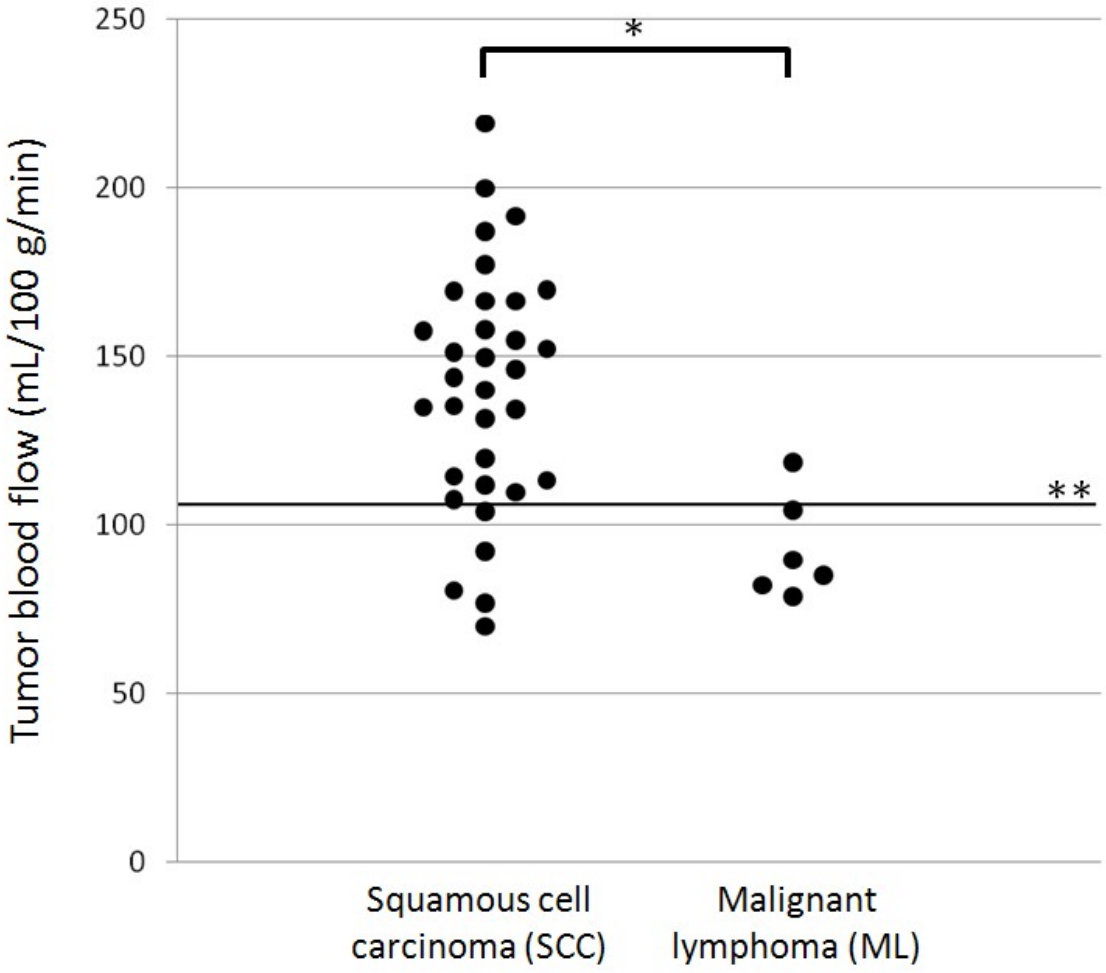
250
200
150
100
50
0
Tumor blood flow (mL/100 g/min)
*
**
Squamous cell carcinoma (SCC)
Malignant lymphoma (ML)

(b)

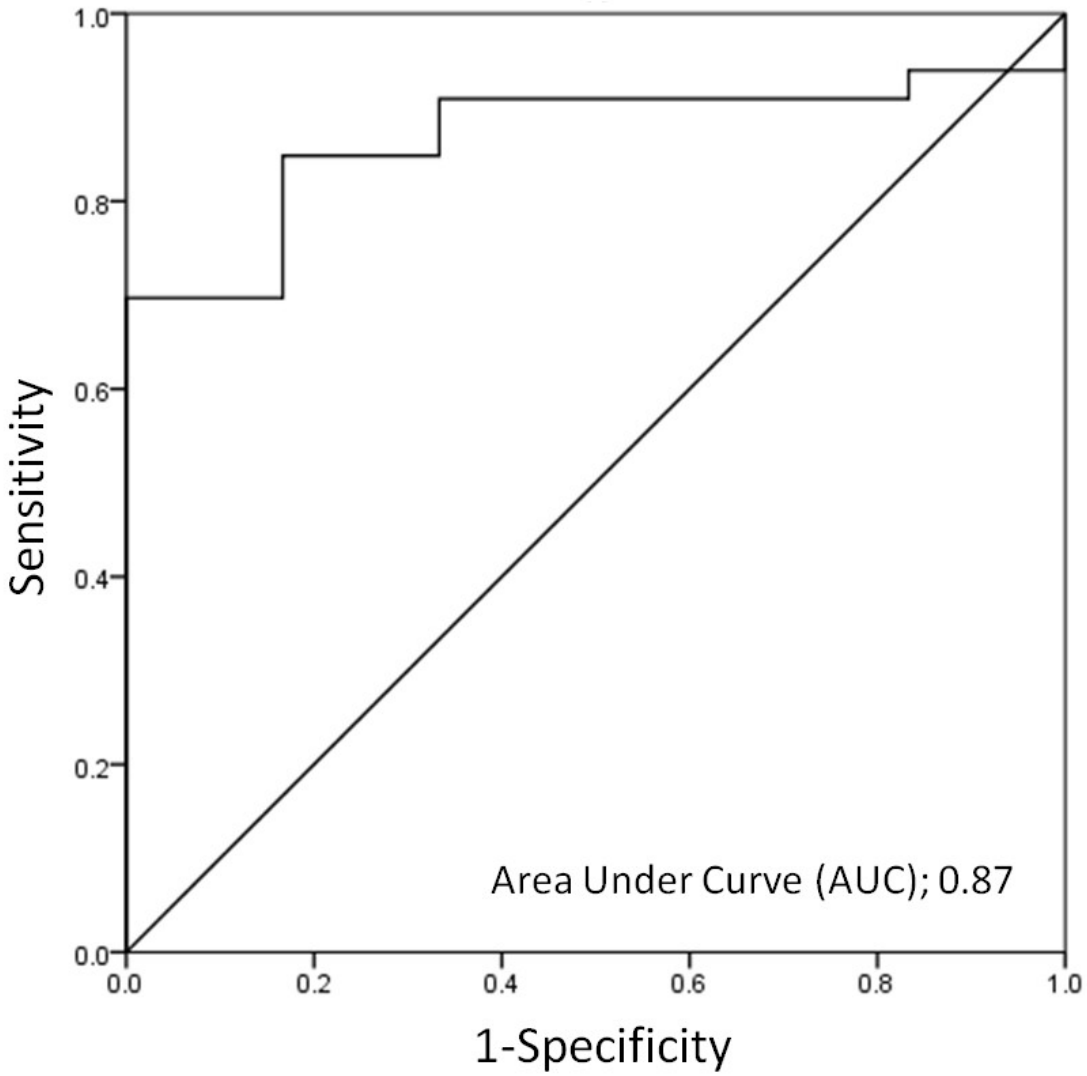

Fig. 3. Histogram CV in the SCC and ML patients.

(a) Histogram CV in patients with SCC or ML. (b) ROC curve for the determination of diagnostic accuracy. There was a significant difference in the CV between the SCC patients (0.45 ± 0.09) and that of the ML patients (0.33 ± 0.04) ($p<0.01$) (*).The ROC

curve analysis revealed the AUC of 0.87 ($p<0.01$) (b), with the best diagnostic accuracy of 0.83 (32/39), sensitivity of 0.82 (27/33), and specificity of 0.83 (5/6), with a threshold value of 0.37 (a, **).

(a)

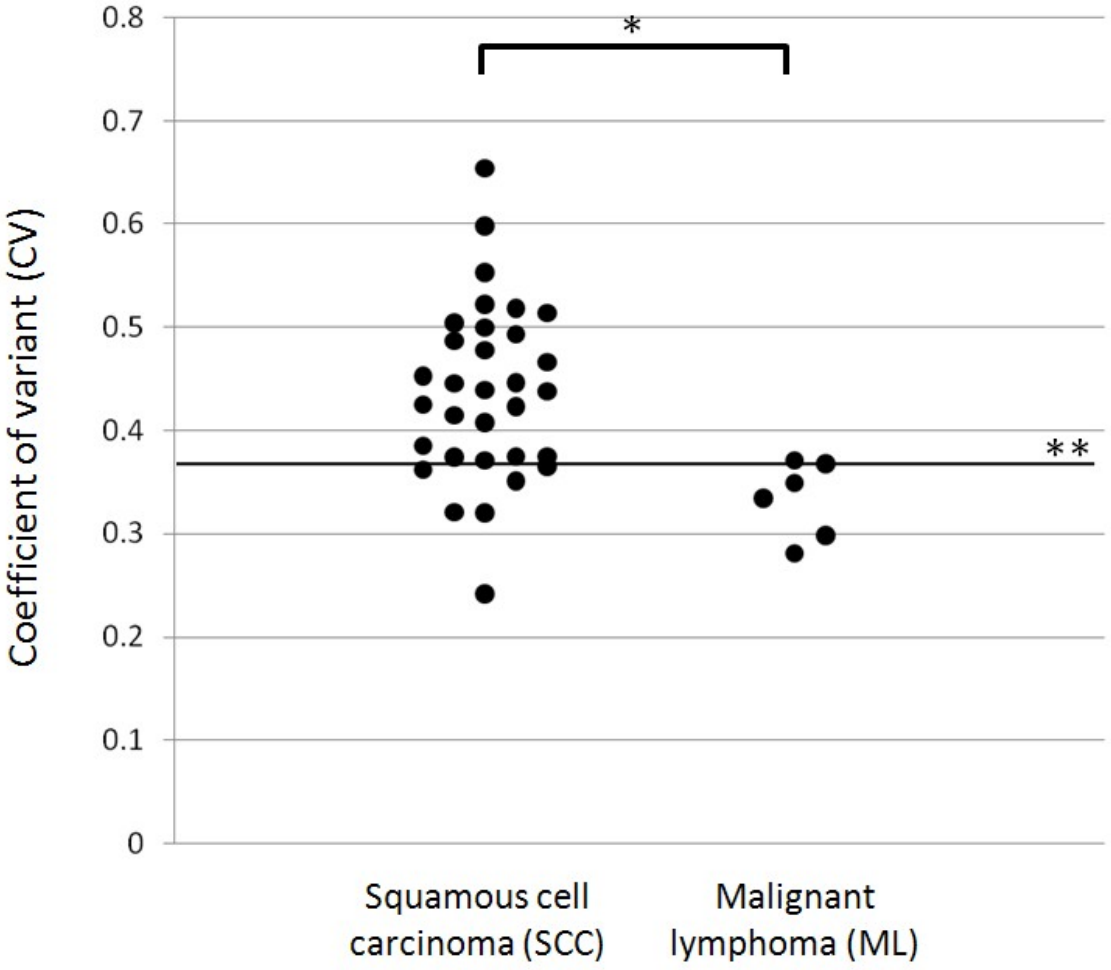

(b)

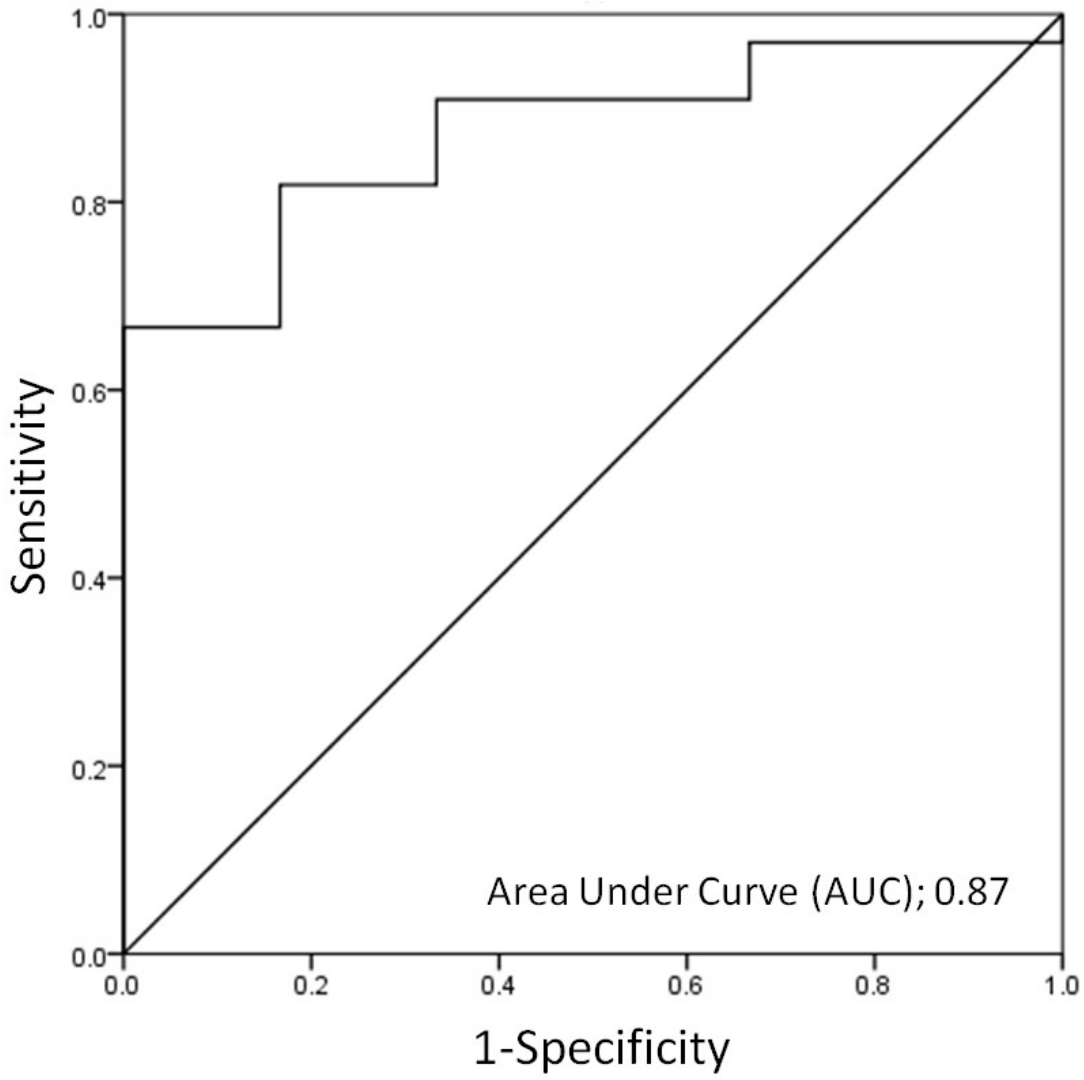

Fig. 4. Histogram kurtosis in the SCC and ML patients.

(a) Histogram kurtosis in patients with SCC or ML. (b) ROC curve for the determination of diagnostic accuracy. There was a significant difference in the histogram kurtosis between the SCC patients (–0.47 ± 0.29) and the ML patients (–0.18

± 0.21) ($p<0.01$) (*).The ROC curve analysis revealed the AUC of 0.78 ($p<0.01$) (b), with the best diagnostic accuracy of 0.67 (26/33), sensitivity of 0.64 (21/33), and specificity of 0.83 (5/6), with a threshold value of −0.39 – −0.40 (a, **).

(a)

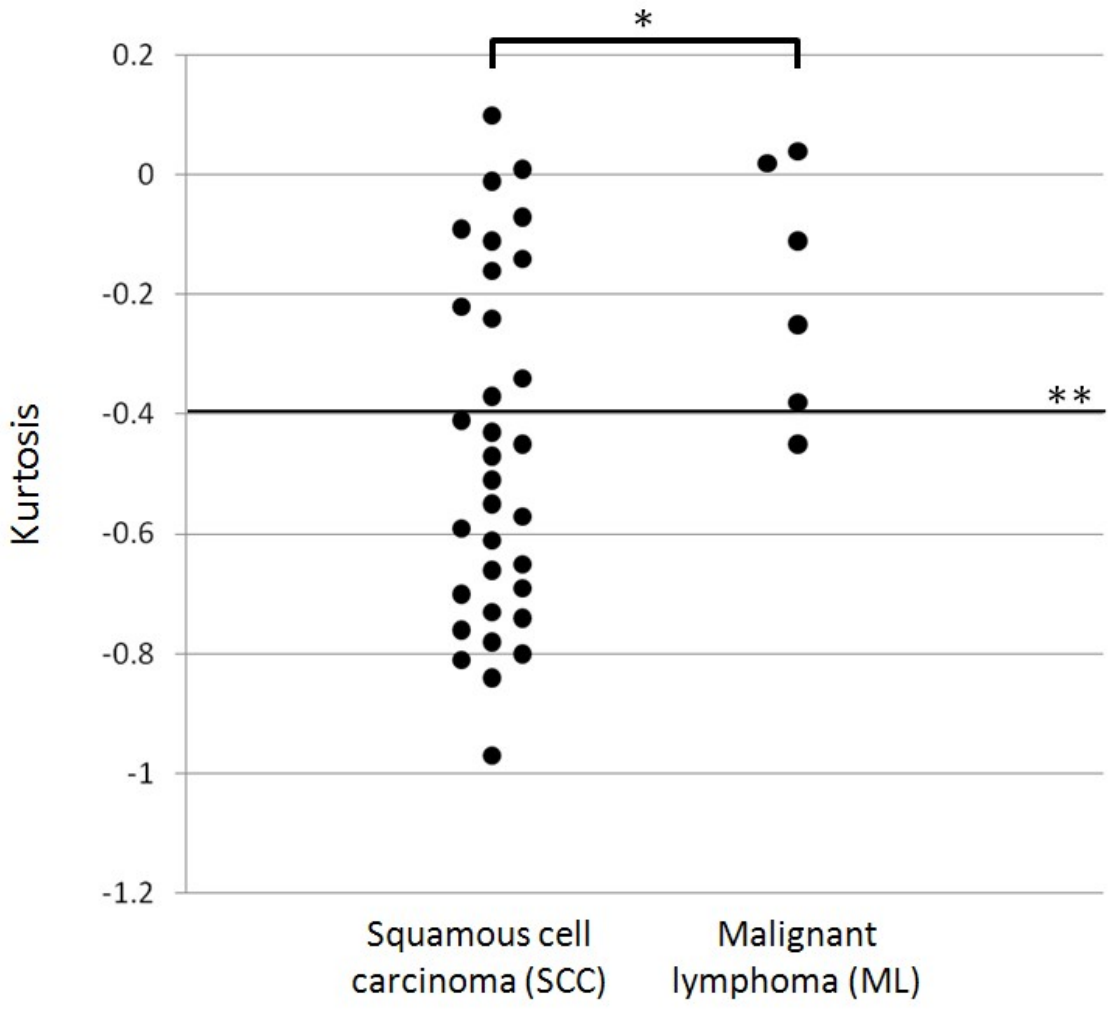

(b)

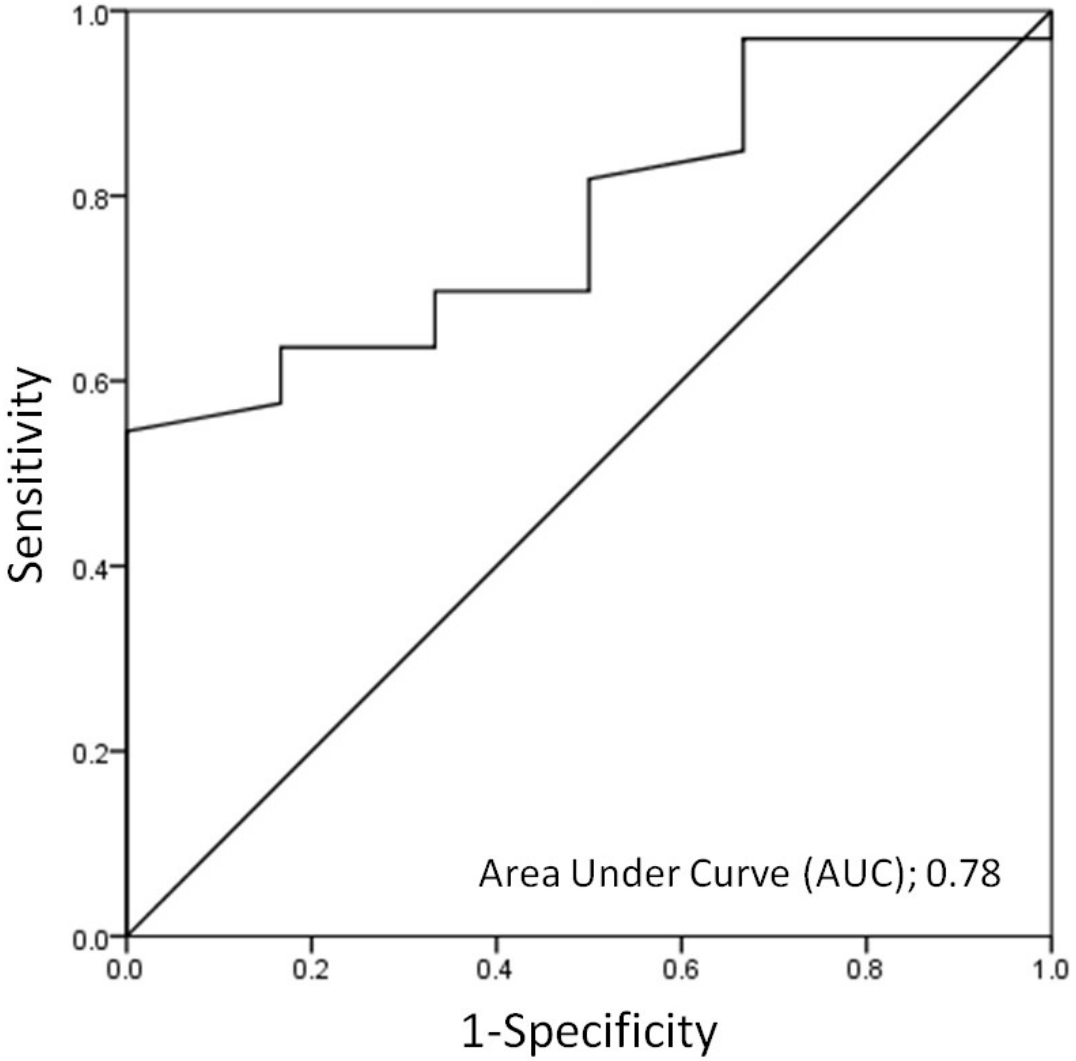

Fig. 5. Histogram skewness in the SCC and ML patients.

No significant difference was observed in the histogram skewness between the patients with SCC and those with ML (p=0.27).

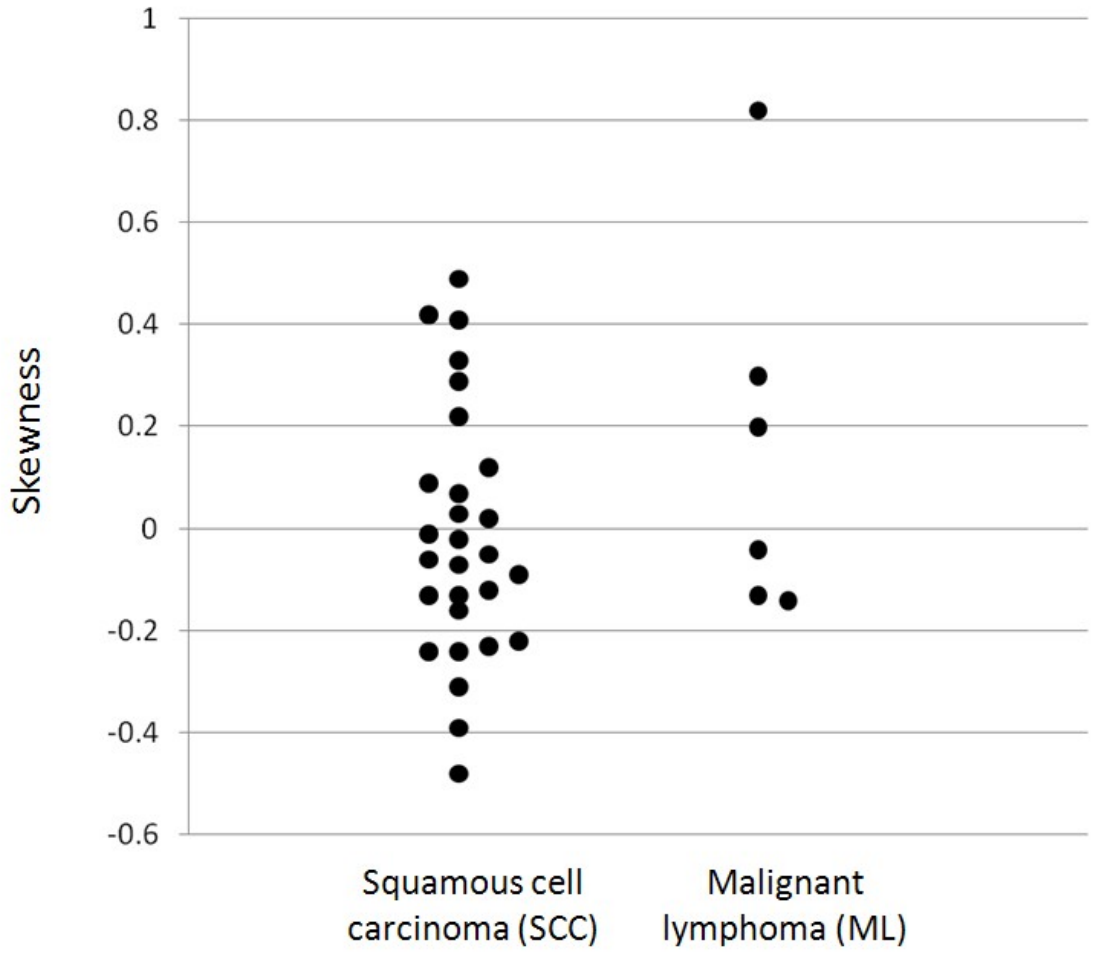

Fig. 6. Two-dimensional plot graph of TBF and histogram CV values.

Two-dimensional plot graph with the percentage change of TV on the vertical axis and the percentage change of TBF on the horizontal axis. When the threshold line was set to 119–134 for TBF (*), 0.37 for histogram CV (**), the sensitivity, specificity and accuracy for the division of SCC and ML were 0.97 (32/33), 1.00 (6/6), and 0.97 (38/39), respectively. With this setting of the threshold for TBF and CV, kurtosis did not

contribute to the diagnostic accuracy.

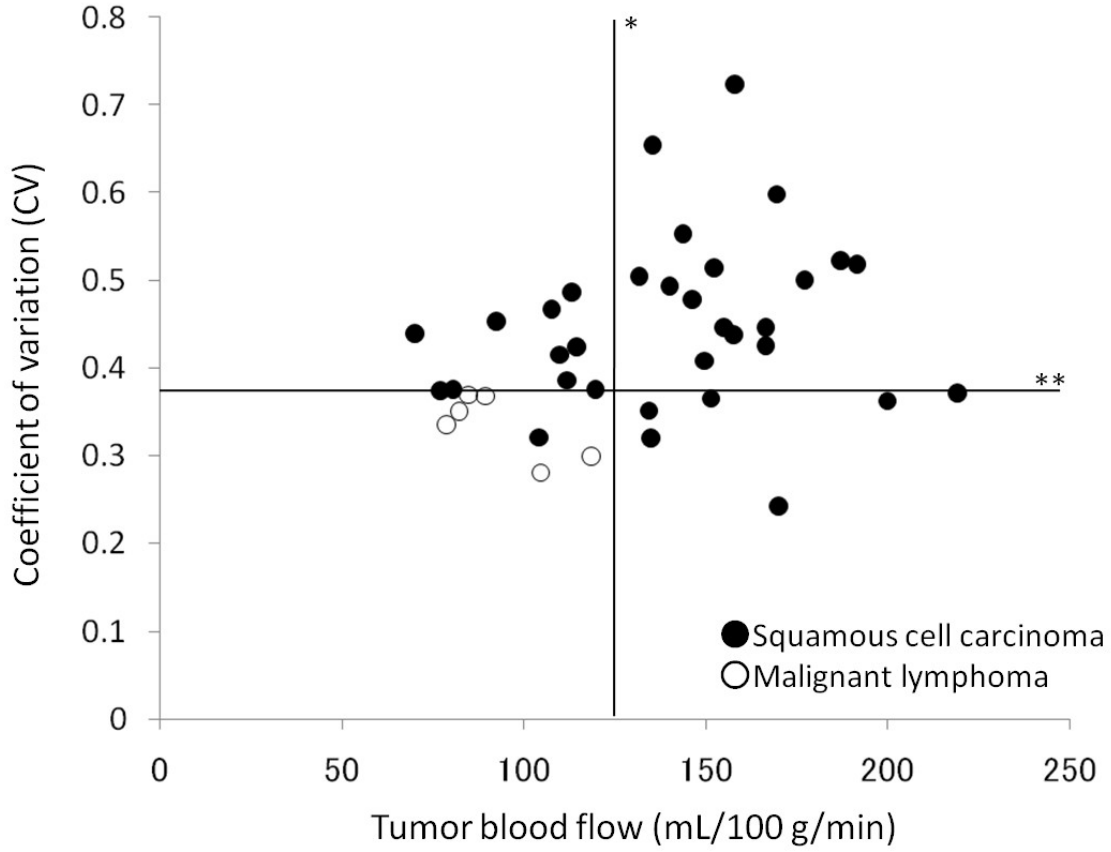

Fig. 7. Case examples of TBF maps of SCC and ML cases.

T2WI and TBF map with the delineated tumor ROI in a patient with SCC (a) and a patient with ML (b). The differentiation was considered difficult from the signal intensity in T2WI only. However, higher TBF and intra-tumoral heterogeneity was clearly observed in the TBF map of the SCC patient (arrow). The measured parameters were: the SCC patient (a), TBF, 169.4 mL/100 g/min; CV, 0.59; kurtosis, −0.66. The ML patient (b), TBF, 104.5 mL/100 g/min; CV, 0.28; kurtosis, 0.04.

(a)

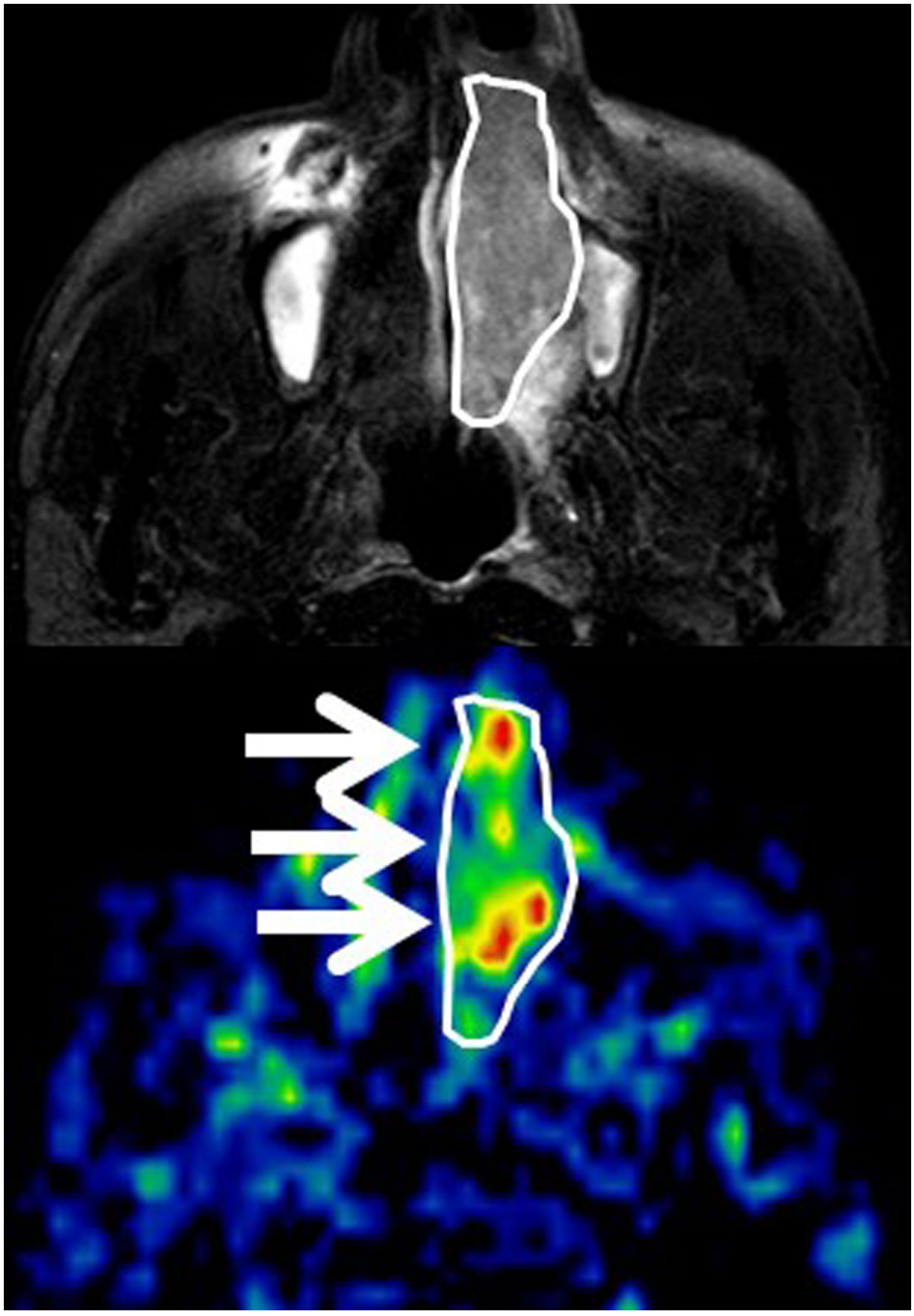

(b)